Entry Mass Transfer in Axial Flows through Randomly Packed Fiber Bundles

L. Bao, B. Liu, and G. G. Lipscomb
Chemical and Environmental Engineering, University of Toledo, Toledo, OH 43606

An analysis of the effects of nonuniform fiber packing on external mass-transfer coefficients for axial flows through bundles of parallel, axially oriented fibers is presented in the entry mass-transfer limit. In this limit, one can obtain an analytic solution to the mass-transfer boundary-layer equations in terms of the velocity gradient on the fiber surface for either a constant wall flux or constant wall concentration. To explicitly calculate mass-transfer coefficients, a numerical approximation for the velocity gradient is obtained from the conservation of momentum equations using the boundary-element method. Results indicate that the effective mass-transfer coefficient depends strongly on fiber packing. Regions of higher fiber packing have lower flows and lower mass-transfer coefficients than regions of lower packing. The net effect is a dramatic decrease in overall mass-transfer coefficient relative to mass-transfer coefficients in regularly packed fiber bundles.

Introduction

Mass transfer in fiber bundles is a problem of great practical importance for membrane separation processes. Such processes commonly utilize a bundle of randomly packed hollow fibers enclosed in a case to contact two process streams. Ports on the case permit one to introduce and remove streams from the space inside the fibers, the lumen, and the space outside the fibers, the shell. Figure 1 illustrates the construction of a typical hollow-fiber membrane module (Lipscomb, 1996).

Hollow-fiber membrane modules are the mass-transfer equivalent of shell and tube heat exchangers. As fluids flow through the lumen and shell, mass is transferred from one stream to the other across the fiber wall. In contrast to heat exchangers, though, mass transfer may involve a combination of diffusion and convection, depending on the nature of the membrane. These modules are used for a wide range of membrane processes, including gas separation, reverse osmosis, filtration, and dialysis (Ho and Sirkar, 1992).

In many cases mass-transfer rates are limited by concentration boundary layers (concentration polarization) that develop in the lumen and shell. The boundary layers are in turn

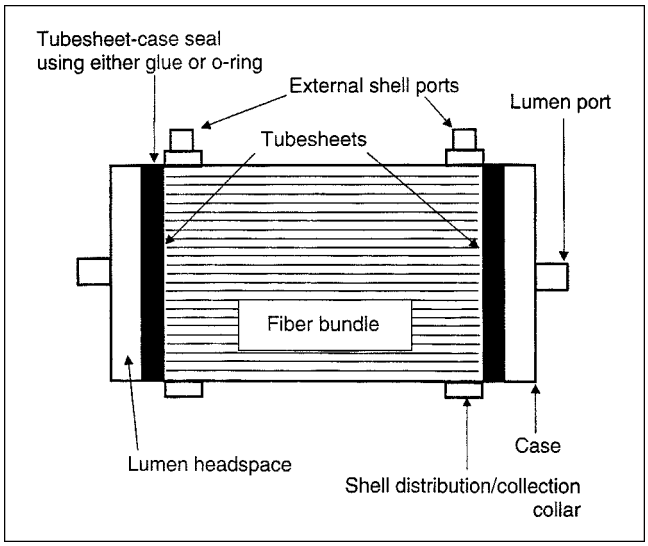

Figure 1. Construction of a typical hollow-fiber membrane module.

The shell distribution/collection collar is typically a channel that extends around the circumference of the module to help ensure axisymmetric fluid distribution around the fiber bundle.

Correspondence concerning this article should be addressed to G. G. Lipscomb.

dependent on the flow through the fiber bundle. The effect of the lumen boundary layer is well understood (Cussler, 1997), but the complicated geometry of randomly packed fiber bundles has frustrated attempts to predict velocity and concentration fields in the shell.

Previous efforts to predict shell velocity and temperature/concentration fields have relied primarily on a number of simplifying assumptions. In an early analysis, Emersleben (1925) studied flow in the low-fiber packing limit where one fiber is immersed in an infinite body of fluid. Happel (1959) introduced the equivalent annulus or free surface approximation, which assumes a cylindrical envelope of fluid surrounds each fiber; the external boundary of this envelope is a line of symmetry. Sparrow and Loeffler (1959) obtained an analytical solution for the well-developed velocity field through infinite arrays of triangular- and square-pitch tube bundles. Noda and Gryte (1979) used this solution to derive an analytic solution for the concentration fields in the well-developed mass-transfer limit. Subsequently, Miyatake and Iwashita (1990, 1991) obtained numerical approximations for the temperature/concentration fields and associated heat/mass-transfer coefficients using the Sparrow and Loeffler velocity fields. Their results span a range of flow rates that encompass both the entry and well-developed mass-transfer limits. Chen and Hlavacek (1994) generalized the equivalent annulus or free surface approximation for use in randomly packed fiber bundles through the use of Voronoi tesselation. Voronoi tesselation surrounds each fiber with a polygonal surface rather than the cylindrical surface of the equivalent annulus approximation. The hydraulic diameter of the enclosed region is used in a correlation for the friction factor to determine flow rates. Rogers and Long (1997) used the same approach to calculate both friction factors and mass-transfer coefficients in randomly packed fiber bundles. Their results indicate that the Voronoi tesselation approach gives a better estimate of module performance than assuming uniform shell flow.

We present here a rigorous analysis of transport in randomly packed fiber bundles that avoids the Voronoi tesselation approximation. The analysis is developed in the entry mass-transfer limit. The results compare well with the numerical results of Miyatake and Iwashita (1990, 1991). To generate randomly packed fiber bundles, we use a periodic medium in which fibers are added to the repeat cell in a random sequential fashion until the target fiber packing is reached. Calculations for the randomly packed fiber bundle indicate that mass-transfer rates can be significantly lower than in regularly packed fiber bundles due to flow maldistribution.

Theory

Figure 2 illustrates the generation of the infinite, spatially periodic medium used to represent the fiber bundle. Fiber packing is specified in a unit cell that is translated in each spatial direction to produce the infinite medium. The unit cell contains multiple fibers that lie parallel to each other and to the z-axis. Because of this alignment, a single x-y cross section of the cell characterizes the entire cell volume. The geometry and value of any field variable at a point (x, y) in the unit cell is the same as at the point $(x \pm il_x, y \pm jl_y)$, where $i, j = 1, 2, 3, \ldots$, and l_x and l_y are the unit cell dimensions in the x and y directions, respectively.

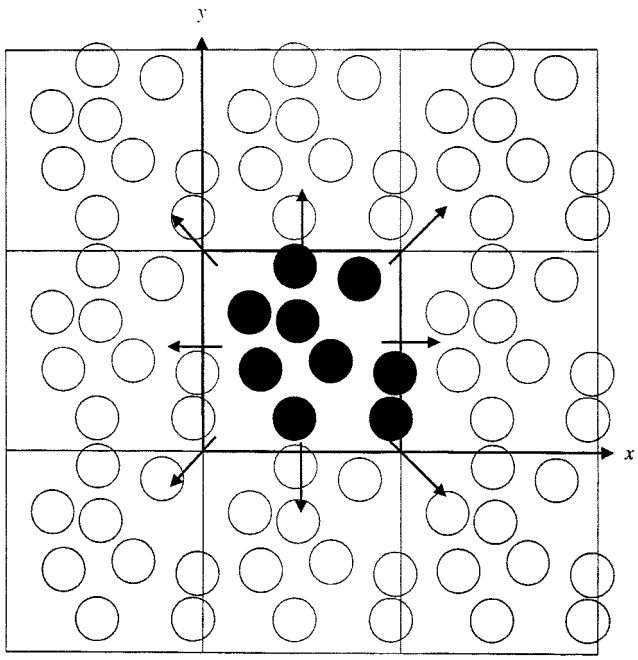

Figure 2. Use of a unit cell to represent an infinite, randomly packed fiber bundle.

The cell is outlined in the center, and fibers with centers in the unit cell have been darkened. The arrows indicate the repetition and translation of the unit cell required to produce an infinite fiber bundle.

Fiber centers are placed on a regular grid to generate regular fiber packings while the locations are selected in a random, sequential fashion to produce random packings. We will use unit cells containing either 9, 16, or 100 fibers and select cell dimensions that yield the desired fiber packing (area occupied by the fiber/total cell area).

One would expect the random media produced by this method to be representative of an infinite random medium only for sufficiently large numbers of fibers in the unit cell or, equivalently, for sufficiently small values of the fiber-diameter to unit-cell dimension ratio. Finite computational resources limit the extent to which this can be achieved, but the algorithms described in the next section could be used for any unit cell size if sufficient computational resources exist.

To simplify the governing conservation equations (Bird et al., 1960), we will make the following assumptions:

1. Flow through the fiber bundle is axial, laminar, and steady.

2. Mass-transfer rates are sufficiently small that flow rates do not change. This would be the case for transport of a dilute solute from the shell fluid to the lumen.

3. Diffusion is Fickian.

4. The concentration or normal concentration gradient along the surface of each fiber is constant.

5. Mass transfer by axial diffusion is negligible relative to axial convection.

6. Fluid material properties are constant.

7. The flow is isothermal.

Based on these assumptions the dimensionless, axial conservation of momentum equation reduces to

$$\frac{\partial^2 v}{\partial x^2} + \frac{\partial^2 v}{\partial y^2} = 1, \tag{1}$$

where v is the dimensionless axial velocity, and x and y are the dimensionless coordinates, respectively. These dimensionless variables are defined in terms of their dimensional values by

$$v = \frac{V}{\frac{R^2}{\mu}\frac{\partial P}{\partial Z}}, \qquad x = \frac{X}{R}, \qquad y = \frac{Y}{R}, \tag{2}$$

where R is the fiber radius, P is the pressure, and μ is the fluid viscosity. The dimensionless conservation of mass equation reduces to

$$v\frac{\partial c}{\partial z} = \frac{\partial^2 c}{\partial x^2} + \frac{\partial^2 c}{\partial y^2}, \tag{3}$$

where the dimensionless axial coordinate z is defined as

$$z = \frac{ZD}{\frac{R^4}{\mu}\frac{\partial P}{\partial Z}}, \tag{4}$$

where D is the diffusion coefficient. We will consider two boundary conditions for the concentration along the fiber surface: constant concentration and constant diffusional flux. The definition of the dimensionless concentration, c, depends on the boundary condition applied. For the constant wall concentration case

$$c = \frac{C - C_w}{C_b - C_w}, \tag{5}$$

while for the constant wall flux case

$$c = \frac{C - C_b}{C_b}, \tag{6}$$

where C_b is the initial bulk fluid concentration and C_w is the wall concentration. Boundary conditions for these equations are

$$c = 1 \quad \text{or} \quad 0, \quad z = 0 \qquad \text{for all } x, y \tag{7}$$

$$v = 0, \quad c = 0 \quad \text{or} \quad \partial c/\partial n = K, \qquad \text{along membrane surface} \tag{8}$$

$$v|_1 = v|_2, \qquad c|_1 = c|_2 \tag{9}$$

$$\left.\frac{\partial v}{\partial n}\right|_1 = -\left.\frac{\partial v}{\partial n}\right|_2, \qquad \left.\frac{\partial c}{\partial n}\right|_1 = -\left.\frac{\partial c}{\partial n}\right|_2$$

where n represents the outward, normal direction to the surface. The first of the two values given in Eqs. 7 and 8 for the concentration boundary condition is for the constant wall concentration case, while the second is for the constant wall flux case. Equation 9 reflects the periodicity of the unit cell: 1 and 2 refer to either the left and right boundaries of the unit cell or the top and bottom boundaries of the unit cell.

To determine mass-transfer rates, one must first solve Eq. 1 for the axial velocity v as a function of position within the cross section of the unit cell. The assumptions of a well-developed velocity field and low mass-transfer rates imply that v is independent of z. Given v one must solve Eq. 3 for the concentration field within the cross section of the unit cell as a function of z. This problem is inherently three-dimensional. Hence, a numerical approximation based on finite differences or finite elements would require discretization of the three-dimensional solution domain. Miyatake and Iwashita (1990, 1991) followed such an approach in their work.

One can avoid the computational complexities associated with a three-dimensional solution in the limit of entry mass transfer. For the entry region, mass transfer produces concentration changes that are confined to a small region adjacent to the fiber surface. In this boundary-layer region, one can assume the velocity varies linearly with distance from the fiber surface where the slope is equal to the velocity gradient, $\partial V/\partial r$. Moreover, one can solve the conservation of mass equation for each fiber independently, since the concentration is uniform and equal to its initial, bulk value in between fibers. The solution given below indicates that although one can solve the conservation of mass equation for each fiber independently, mass transfer to a given fiber is affected by the presence of other fibers through the value of the surface-velocity gradient.

For a given fiber, the conservation of mass equation in a cylindrical coordinate system located at the fiber center is

$$\dot{\gamma}\xi\frac{\partial c}{\partial z} = \frac{\partial^2 c}{\partial \xi^2} + \frac{1}{(\xi+1)}\frac{\partial c}{\partial \xi} + \frac{1}{(\xi+1)^2}\frac{\partial^2 c}{\partial \theta^2}, \tag{10}$$

where ξ is the dimensionless distance from the fiber surface, $\xi = (r/R) - 1$, and the axial velocity has been replaced by its linear approximation near the fiber surface. Note that $\dot{\gamma} = \partial v/\partial \xi$ is a function of θ.

One can further simplify Eq. 10 through an order-of-magnitude analysis of each term. Assuming that most concentration changes occur within a thin boundary and scaling ξ with this boundary layer thickness, one can argue the last two terms on the righthand side of Eq. 10 are negligible relative to the first term on the righthand side. Neglecting these terms gives

$$\dot{\gamma}\xi\frac{\partial c}{\partial z} = \frac{\partial^2 c}{\partial \xi^2}, \tag{11}$$

and the boundary conditions become

$$c = 0 \quad \text{or} \quad \partial c/\partial n = K, \qquad \xi = 0 \tag{12}$$

$$c \to 1 \quad \text{or} \quad c \to 0, \qquad \xi \to \infty. \tag{13}$$

Equations 11–13 are identical to the boundary-layer equa-

tions for a flat plate, and their solution is readily found using a similarity transformation (Leal, 1992). Since the solution depends on $\dot{\gamma}$, the concentration field and diffusion flux will also be functions of θ. One can calculate an effective, local mass-transfer coefficient, k, for the entire unit cell from an overall mass balance. Equating the product of mass-transfer coefficient, mass-transfer area, and average concentration difference to the diffusional flux gives

$$k(2\pi RN)\frac{\sum_{i=1}^{N}\int_0^{2\pi}(C_b - C_w)_i R\, d\theta}{2\pi RN} = \sum_{i=1}^{N}\int_0^{2\pi} D(\partial C/\partial r)_{w,i}\, R\, d\theta, \quad (14)$$

where N is the number of fibers in the unit cell. Equation 14 can be rewritten in terms of the local Sherwood number as

$$Sh_{\text{loc}} = \frac{2Rk}{D} = 2\frac{\sum_{i=1}^{N}\int_0^{2\pi}(\partial c/\partial \xi)_{w,i} d\theta}{\sum_{i=1}^{N}\int_0^{2\pi}(c_b - c_w)_i d\theta}. \quad (15)$$

Substituting the solution for the concentration field for the constant wall concentration case into Eq. 15 gives

$$Sh_{\text{loc},c} = \frac{2Rk}{D} = \frac{2}{\Gamma(4/3)}\frac{\overline{(\dot{\gamma})_w^{1/3}}}{(9q)^{1/3}} Gz^{1/3} = \alpha_c Gz^{1/3}, \quad (16)$$

where the overbar indicates an average over the fiber surface area available for mass transfer defined as

$$\overline{(\dot{\gamma})_w^{1/3}} = \frac{\sum_{i=1}^{N}\int_0^{2\pi}(\dot{\gamma})_{w,i}^{1/3} d\theta}{2\pi N}; \quad (17)$$

N is the number of fibers in the unit cell; q is the dimensionless flow rate per fiber defined as

$$q = \frac{Q}{\frac{R^4}{\mu}\frac{\partial p}{\partial Z}}, \quad (18)$$

Q is the flow rate per fiber; Gz is the Graetz number defined as

$$Gz = \frac{Q}{DZ}; \quad (19)$$

and Z is the distance from the origin along the z-axis. The dimensionless velocity is the solution to Eq. 1, subject to boundary conditions given by Eqs. 8–9, which are independent of pressure gradient and fluid viscosity. Thus, the dimensionless flow rate per fiber and α_c, which are calculated from it, depend only on the geometry of the unit cell. Equation 16 is identical to that presented by Miyatake and Iwashita (1990) in their calculations for square and triangular arrays with a constant surface temperature/concentration boundary condition.

Substituting the solution for the concentration field for the constant wall flux case into Eq. 15 gives

$$Sh_{\text{loc},f} = \frac{2Rk}{D} = \frac{2\Gamma(2/3)}{(9q)^{1/3}}\frac{1}{\overline{(\dot{\gamma})_w^{-1/3}}} Gz^{1/3} = \alpha_f Gz^{1/3}. \quad (20)$$

Equation 20 is identical to that used by Miyatake and Iwashita (1991) for a constant wall flux boundary condition.

Equations 16 and 20 are also applicable for flow within a pipe, if one substitutes appropriate values for the velocity gradient normal to the pipe wall and the dimensionless flow rate. Doing so gives $\alpha_c = 2(2/9)^{1/3}/\Gamma(4/3) = 1.357$ and $\alpha_f = 2(2/9)^{1/3}\Gamma(4/3) = 1.640$, which are identical to the values reported in the literature (Deen, 1998). To obtain effective mass-transfer coefficients over a length L of fiber, one must integrate the local mass-transfer coefficients with respect to Z and divide by L. This introduces an additional factor of 3/2 that multiplies the righthand side of Eqs. 16 and 20.

The mass-transfer coefficients given by Eqs. 16 and 20 were obtained by solving the conservation-of-mass equation for each fiber independently in the entry mass-transfer limit. However, as noted earlier, mass transfer to individual fibers and overall mass transfer are affected by interfiber interactions through the value of the surface-velocity gradient required to evaluate these expressions. This effect is responsible for the variation in mass-transfer coefficients with fiber packing reported by Miyatake and Iwashita for regular fiber packings and the variations reported here for random fiber packings.

To evaluate the surface-velocity gradient, we use the boundary-element method (Brebbia et al., 1984). The boundary-element method uses the fundamental solution of a differential equation to transform it into an integral equation over the boundary of the solution domain. This reduces the dimensionality of the problem by one. In our work, the problem of determining the velocity in two-dimensions (x and y) is reduced to the problem of determining the velocity or normal velocity gradient in one-dimension (along the boundary of the solution domain).

The integral equation is solved by discretizing the boundary into a finite number of segments and determining velocity and velocity gradients for each segment. We use constant value elements here. An algebraic equation for the unknown value of velocity or velocity gradient on each segment is obtained by evaluating the integral equation using numerical quadrature; the singular integral over the segment itself is evaluated analytically. To evaluate discretization error, simulations were run with 450 to 750 elements. The results indicate that error in the calculated mass-transfer coefficients is less than 5%.

Once the boundary values for velocity and velocity gradient are known, one can calculate the velocity field within the solution domain. The dimensionless flow rate, q, is calculated by discretizing the solution domain and calculating the velocity at each nodal point. The flow rate is calculated by numeri-

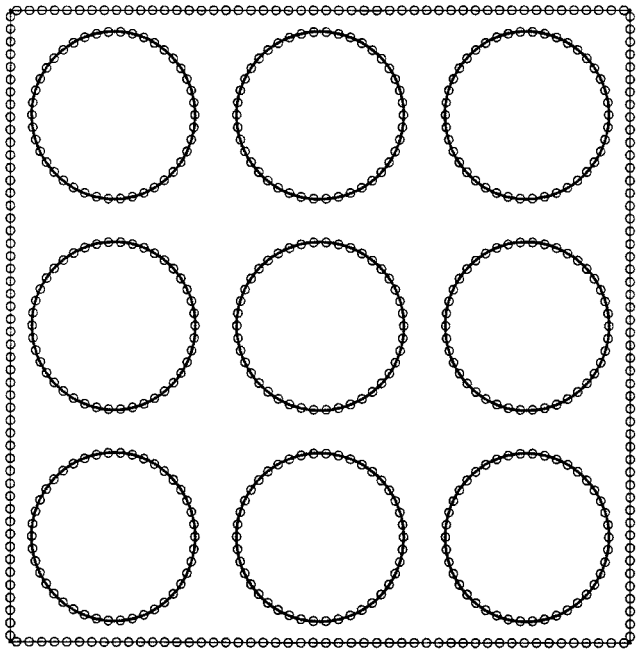

Figure 3. Typical boundary discretization used to solve for the velocity field within a square fiber array.

The fiber packing fraction is 0.5. The circles indicate the midpoint of each element.

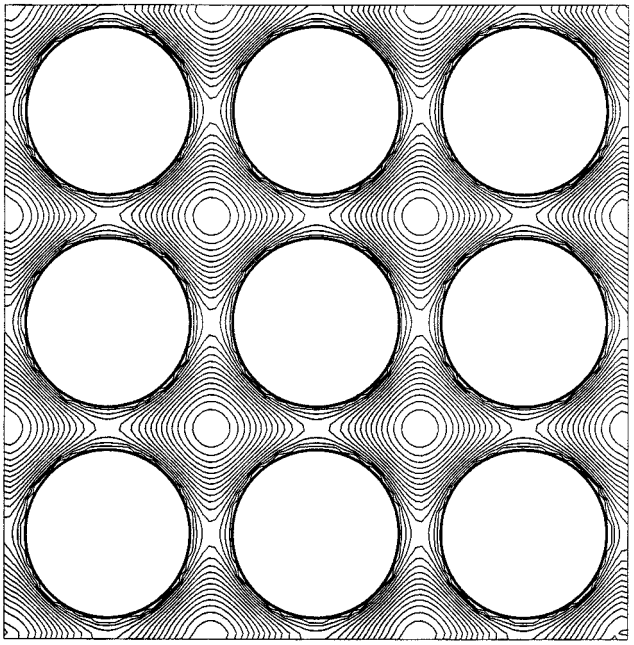

Figure 4. Contours of constant velocity within a square fiber array; the increment between contour lines is 0.012.

cally integrating over the grid. This process can be simplified by using a uniform grid, setting the velocity for grid points inside a fiber to zero, and integrating over the entire unit cell including the fibers themselves. For a sufficiently fine grid, this will yield the same result as discretizing and integrating over the solution domain only. Finally, values for α_c and α_f are calculated from Eqs. 16 and 20, respectively.

The boundary element method offers two principal advantages over alternative-solution algorithms. First, one of the primary solution variables is the normal velocity gradient that is required to calculate mass-transfer coefficients. In finite difference or finite-element algorithms the velocity is the primary solution variable, and one must differentiate the result to obtain the velocity gradient, which can introduce numerical error. Second, discretization of the solution domain is simpler, since only the boundary must be discretized to solve for the velocity field; the entire domain must be discretized to calculate q, but this process can be simplified as described earlier.

Results

To evaluate the numerical algorithm, values for α_c and α_f were calculated for regular square and triangular arrays. Figure 3 illustrates a typical boundary discretization for a square array with 50% fiber packing (total fiber cross-sectional area/unit cell cross-sectional area). Figure 4 illustrates the computed velocity field. Note the uniform flow in between fibers.

Table 1 gives the values computed for α_c as a function of fiber packing for square and triangular arrays. Table 1 also contains values for α_c taken from Miyatake and Iwashita (1990) and calculated from Eq. 16 using the analytic solution for the velocity field (Sparrow and Loeffler, 1959). The agreement between the boundary-element results, the analytic solution, and the results of Miyatake and Iwashita is excellent.

Figure 5 illustrates the predicted variation of Sh with Gz for square arrays with a constant wall concentration. The results of Miyatake and Iwashita are also shown. The entry mass-transfer results appear to provide good predictions of Sh for $Gz > 1000$. For smaller Gz, deviations become significant as the well-developed mass-transfer limit is approached. The same conclusions apply for triangular arrays as indicated by Figure 6.

Table 2 gives the values computed for α_f as a function of fiber packing for square and triangular arrays. As observed for α_c, the results are in excellent agreement with the analytic solution and the results of Miyatake and Iwashita (1991).

Table 1. Variation of α_c with Fiber Packing Fraction for Square and Triangular Arrays

Square Array				Triangular Array			
ϕ	This Work	Analytic	Miyatake–Iwashita (1990)	ϕ	This Work	Analytic	Miyatake–Iwashita (1990)
0.755	1.84	1.85	1.84	0.872	3.50	3.49	3.51
0.712	1.80	1.80	1.81	0.823	3.15	3.15	3.15
0.649	1.67	1.67	1.68	0.750	2.61	2.61	2.56
0.545	1.41	1.41	1.41	0.630	1.93	1.93	1.88
0.349	0.946	0.946	0.939	0.403	1.12	1.12	1.11
0.196	0.621	0.621	0.617	0.227	0.696	0.695	0.708
0.0491	0.283	0.283	0.279	0.0567	0.306	0.306	0.315

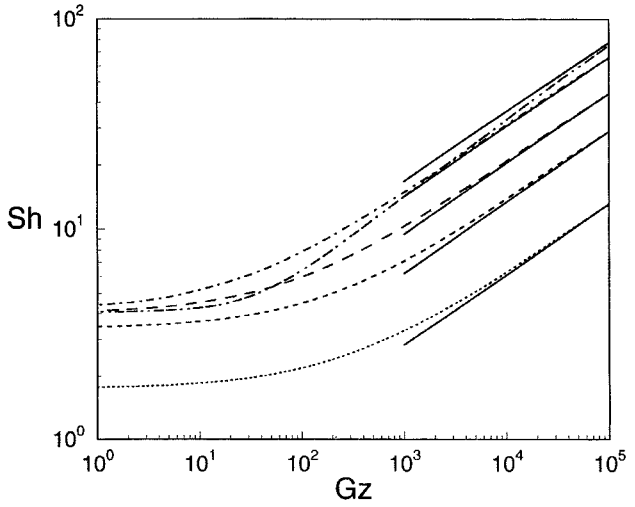

Figure 5. Comparison of the predicted relationship between $Sh_{loc,c}$ and Gz with the results of Miyatake and Iwashita (1990) for square fiber arrays.

The solid lines indicate the present work, which is valid only for large Gz. The curves correspond to the following fiber-packing fractions: 0.049—dot; 0.20—short dash; 0.35—long dash; 0.55—dash–dot; 0.65—double dash–double dot.

Such good agreement demonstrates that discretization error can be reduced to less than 1% in the calculation of mass-transfer coefficients.

Figure 7 illustrates the boundary discretization for one unit cell used to represent a randomly packed fiber bundle with 50% fiber packing. Figure 8 illustrates a typical computed

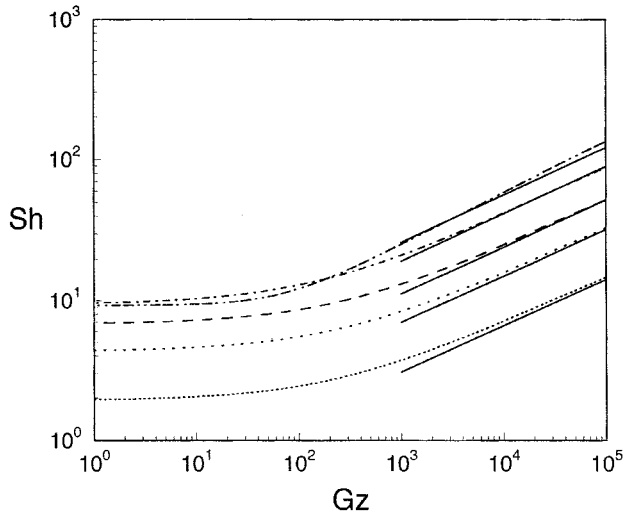

Figure 6. Comparison of the predicted relationship between $Sh_{loc,c}$ and Gz with the results of Miyatake and Iwashita (1990) for triangular fiber arrays.

The solid lines indicate the present work, which is valid only for large Gz. The curves correspond to the following fiber-packing fractions: 0.057—dot; 0.23—short dash; 0.40—long dash; 0.63—dash–dot; 0.75—double dash–double dot.

Table 2. Variation of α_f with Fiber Packing Fraction for Square and Triangular Fiber Arrays

Square Array				Triangular Array			
ϕ	This Work	Analytic	Miyatake–Iwashita (1991)	ϕ	This Work	Analytic	Miyatake–Iwashita (1991)
0.755	1.99	2.01	2.06	0.872	4.02	4.01	4.06
0.712	2.07	2.07	2.06	0.823	3.74	3.73	3.64
0.649	1.97	1.97	1.92	0.750	3.14	3.13	3.02
0.545	1.70	1.70	1.63	0.630	2.33	2.33	2.28
0.349	1.14	1.14	1.14	0.403	1.35	1.35	1.39
0.196	0.750	0.750	0.771	0.227	0.841	0.841	0.874
0.0491	0.342	0.342	0.348	0.0567	0.369	0.370	0.369

velocity field. Figures 7 and 8 show two different unit cells and provide an indication of the variation in fiber packing that occurs.

In contrast to Figure 4, Figure 8 indicates that flow through the randomly packed fiber bundle can be highly nonuniform. Fluid velocities in regions where fiber spacing is less than average are much lower than velocities through regions where fiber spacing is greater than average. One can rationalize such a strong dependence by noting that the flow rate through a closed channel is proportional to the fourth power of the hydraulic diameter according to the Hagen-Poiseuille law (Bird et al., 1960).

Regions where fibers come in close contact are essentially stagnant, so the fiber surface area surrounding such regions is not utilized for mass transfer. However, in regions where fibers are further apart, higher flows will lead to higher sur-

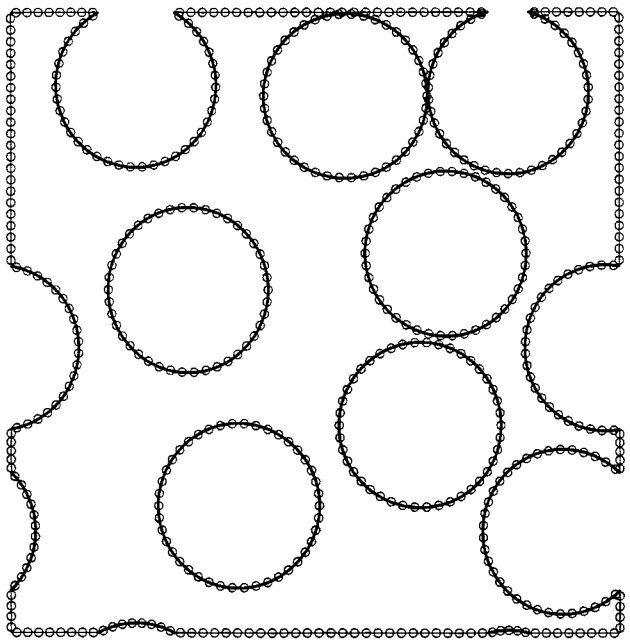

Figure 7. Typical boundary discretization used to solve for the velocity field within a randomly packed fiber bundle.

The fiber-packing fraction is 0.5. The circles indicate the midpoint of linear element.

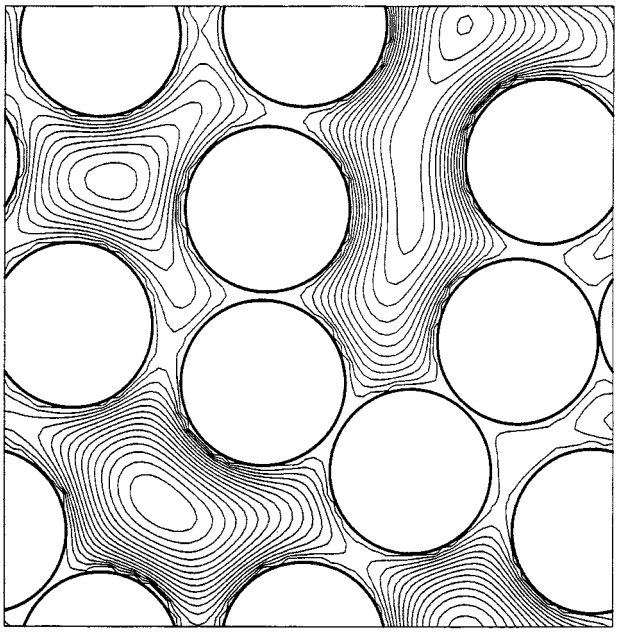

Figure 8. Contours of constant velocity within a randomly packed fiber bundle; the increment between contour lines is 0.012.

face-velocity gradients. Thus, mass-transfer coefficients will be higher in these regions. The increase in mass-transfer coefficient is partially offset by a reduction in the surface-area-to-flow-rate ratio. The overall mass-transfer coefficient will reflect the relative contribution of these opposing effects.

Figures 9 and 10 illustrate the dependence of α_c and α_f, respectively, on fiber packing. Mass-transfer coefficients for random packings are smaller than those for regular packings. On a percentage basis, the reduction appears to be a maximum for fiber packings around 50% where the effective value

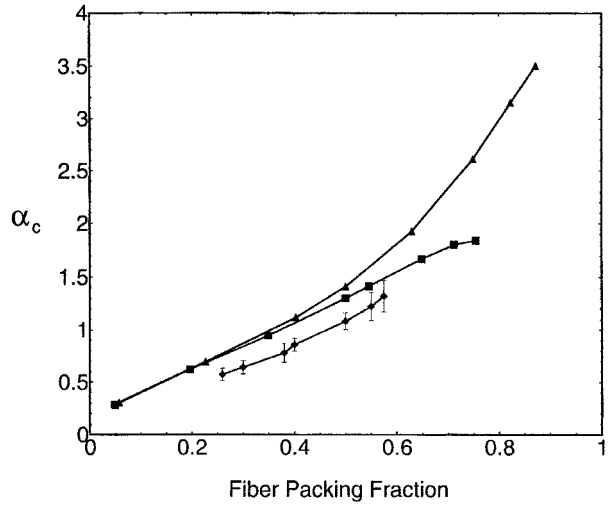

Figure 9. Variation of α_c with fiber-packing fraction.

■—square array; ▲—triangular array; ♦—random packing; the range of values is also indicated for the random packing results.

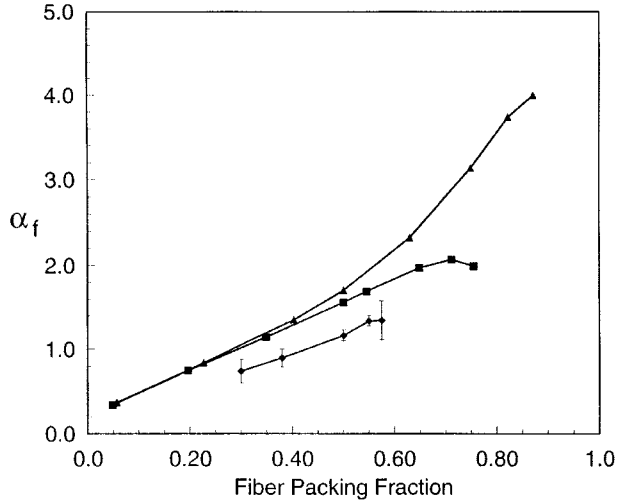

Figure 10. Variation of α_f with fiber-packing fraction.

■—square array; ▲—triangular array; ♦—random packing; the range of values is also indicated for the random packing results.

of *Sh* is ~75% of the value for an equivalent square array and ~70% of the value for an equivalent triangular array.

The reduction in *Sh* is smaller for lower and higher fiber packings. In the low packing limit, one would expect all three results to approach the same asymptotic value, since each fiber would appear to exist by itself in an infinite, unbounded fluid. In the high packing limit, variations in interfiber spacing become smaller, so one might expect less deviation from regular packings.

Figures 9 and 10 also indicate the range of values for α_c and α_f calculated for different randomly packed unit cells. To evaluate the effects of random packing, a number of cells must be generated and the associated mass-transfer coefficients evaluated. Averaging the values for each cell gives an average mass-transfer coefficient for the bundle. For the results presented here, at least 5 cells were used for the α_f calculations, and at least 10 cells for the α_c calculations. Table 3 gives the minimum, maximum, and average values calculated for α_c and α_f. The difference between the maximum and minimum values can be as large as 30% of the average. This indicates that local variations in fiber packing can have a dramatic impact on mass transfer.

The results presented in Figures 9 and 10 were obtained using nine fibers per unit cell. To evaluate the effect of fiber number, we performed calculations using 16 and 100 fibers per cell. Cells containing 16 fibers were used for packing fractions of 26 and 50%, while cells containing 100 fibers were used for typical commercial packing fractions of 50%. The results are given in Table 3. A Student's *t*-test (McBean and Rovers, 1998) of the values calculated for α_c and α_f at 26% packing shows no significant difference between the results obtained using 9 and 16 fibers at the 95% confidence level. An analysis of the variance (ANOVA; McBean and Rovers, 1998) of the values calculated for α_c and α_f at 50% packing also shows no significant difference between the results obtained using 9, 16, and 100 fibers at the 95% confidence level. Therefore, we believe the results obtained using nine fibers are representative of mass transfer in random fiber bundles.

Table 3. Variation of α_c and α_f Among the Unit Cells Used to Simulate Random Fiber Packing

ϕ	Unit Cell Fiber No.	α_c Min.	α_c Max.	α_c Avg.	α_f Min.	α_f Max.	α_f Avg.
0.26	9	0.514	0.613	0.573	0.581	0.848	0.694
0.26	16	0.433	0.636	0.544	0.564	0.731	0.640
0.30	9	0.580	0.709	0.643	0.604	0.808	0.742
0.38	9	0.688	0.856	0.780	0.793	1.00	0.899
0.40	9	0.799	0.889	0.860	—	—	—
0.50	9	0.971	1.19	1.08	1.08	1.43	1.25
0.50	16	1.01	1.21	1.08	1.09	1.31	1.20
0.50	100	1.12	1.15	1.14	1.23	1.28	1.27
0.55	9	1.09	1.33	1.22	1.28	1.40	1.34
0.575	9	1.17	1.46	1.32	1.11	1.53	1.35

The effect of randomness in fiber packing on effective external mass-transfer coefficients is similar to the effect reported for variation in fiber size on internal mass-transfer coefficients (Elmore and Lipscomb, 1995). A variation in fiber size has a detrimental impact on performance; variation in other membrane properties such as permeability may result in a slight enhancement of mass transfer (Crowder and Cussler, 1997). Larger-diameter fibers behave like regions with larger than average interfiber spacing; flows are higher and mass-transfer coefficients are higher, but the surface area available for mass transfer per unit volume is lower. Smaller fibers behave like regions with smaller than average interfiber spacing: flows are lower and mass-transfer coefficients are lower. The cumulative effect of these changes is a reduction in mass-transfer coefficient.

The literature contains numerous correlations for shell-side mass-transfer coefficients (Ho and Sirkar, 1992). Three representative relationships are Yang and Cussler (1986):

$$Sh_{lm} = 1.25\left(\frac{1-\phi}{\phi}\right)^{0.86}\left(\frac{2R}{L}\right)^{0.93} Re^{0.93}Sc^{0.33}, \quad (21)$$

Prasad and Sirkar (1988):

$$Sh_{lm} = 5.85(1-\phi)\left(\frac{1-\phi}{\phi}\right)^{0.66}\left(\frac{2R}{L}\right) Re^{0.66}Sc^{0.33}, \quad (22)$$

Costello et al. (1993):

$$Sh_{lm} = 0.53(1-1.1\phi)\left(\frac{1-\phi}{\phi}\right)^{-0.47} Re^{0.53}Sc^{0.33}, \quad (23)$$

where Sh_{lm} is the Sherwood number, as defined in Eq. 16, calculated using the effective mass-transfer coefficient for a module length L (the subscript lm indicates the logarithmic mean value); ϕ is the fiber packing fraction; Sc is the Schmidt number (ν/D); Re is the Reynolds number defined as

$$Re = \frac{2RV_b}{\nu}; \quad (24)$$

and ν is the kinematic viscosity. The range of values for ϕ, Re, and Sc for which the correlations given by Eqs. 21–23 were developed are given in Table 4. In terms of Re and Sc, Eqs. 16 and 20 become

$$Sh_{lm,c} = 1.38(-0.07+2.35\phi)\left(\frac{1-\phi}{\phi}\right)^{1/3}\left(\frac{2R}{L}\right)^{1/3} Re^{1/3}Sc^{1/3} \quad (25)$$

$$Sh_{lm,f} = 1.38(0.04+2.29\phi)\left(\frac{1-\phi}{\phi}\right)^{1/3}\left(\frac{2R}{L}\right)^{1/3} Re^{1/3}Sc^{1/3}, \quad (26)$$

where the righthand sides of Eqs. 16 and 20 have been multiplied by 3/2 to give the effective mass-transfer coefficient over a module length L, and linear regression was used to obtain expressions for α as a function of ϕ for $0.26 < \phi < 0.575$.

In comparison to our results, several significant differences exist. First, Sh does not vary with Re raised to the 1/3 power in any of the correlations. Second, Eqs. 21 and 23 predict significantly higher mass-transfer coefficients than predicted for random and regular fiber packings. This is illustrated in Figure 11, where values of Sh as a function of Re for $Sc =$ 1,000 and 26% fiber packing are shown. Third, Eqs. 22 and 23 predict a different dependence of mass-transfer coefficient on fiber packing. For example, as illustrated in Figure 12 for $Re = 450$ and $Sc = 1{,}000$, the literature correlations predict a *decrease* in mass-transfer coefficient with increasing fiber packing, while the results for random and regular fiber packings predict a monotonic *increase*.

Why do such significant differences exist between our results and the literature and within the literature itself? We believe several factors are responsible for these differences. Much of the prior work was conducted with modules contain-

Table 4. Range of Conditions Used to Obtain Literature Shell-Side Mass-Transfer Coefficient Correlations

Correlation	$100^*\phi$	$Re(1-\phi)/\phi$	Sc
Yang and Cussler (1986)	3–26	0.5–500	~ 500
Prasad and Sirkar (1988)	4–40	0–500	300–1,000
Costello et al. (1993)	30–75	20–350	~ 500

Note that the factor $(1-\phi)/\phi$ is equal to the ratio of the hydraulic diameter to the fiber diameter.

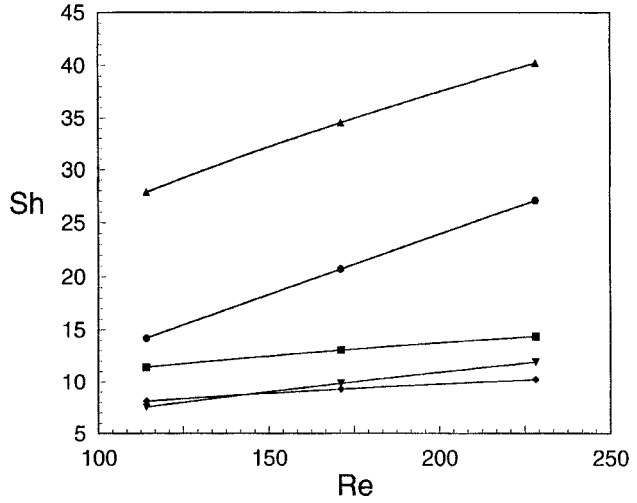

Figure 11. Dependence of Sh_{lm} on Re for $Sc = 1{,}000$, $2R/L = 0.0039$, and $\phi = 0.26$ as predicted by various correlations.

◆—random packing, constant wall concentration; ■—square array; ●—Yang and Cussler (1986); ▲—Costello et al. (1993); ▼—Prasad and Sirkar (1988).

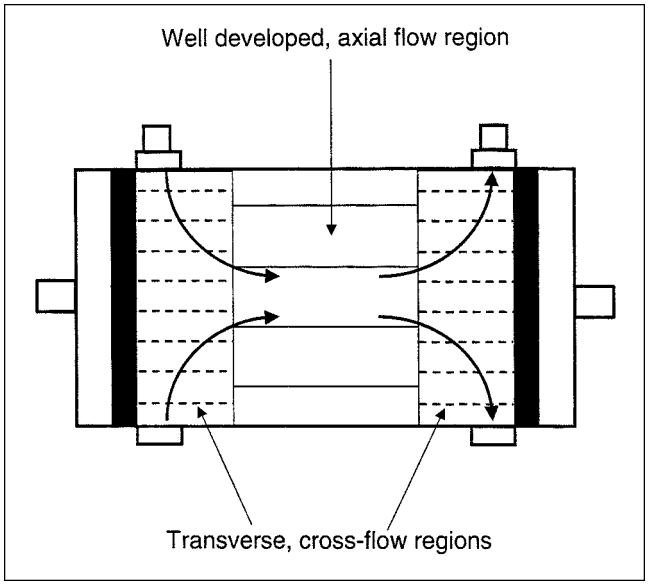

Figure 13. Fluid distribution regions near shell inlet and outlet ports where fluid flow is primarily transverse to the fiber bundle.

ing relatively small numbers of fibers. Moreover, many of the modules were constructed by hand following some unspecified manufacturing protocol. While one would expect accurate reporting of fiber packing for such units, it is more difficult to assess how well the shell fluid introduction and removal ports were designed. If the ports are not designed well, the region where the fluid is distributed across the fiber bundle (and collected at the opposite end) can extend over a significant portion of the module (see Figure 13). Moreover, if fibers are not parallel within the bundle, axial flow channels can end or split to promote additional flow across fibers rather than along them (Costello et al., 1993). One would expect these *cross-flow* regions to have higher mass-transfer coefficients (Wickramasinghe et al., 1992) and, potentially, increase the effective value for the module. Additionally, some designs might produce unexpected secondary flows that enhance mass transfer as speculated previously (Yang and Cussler, 1986).

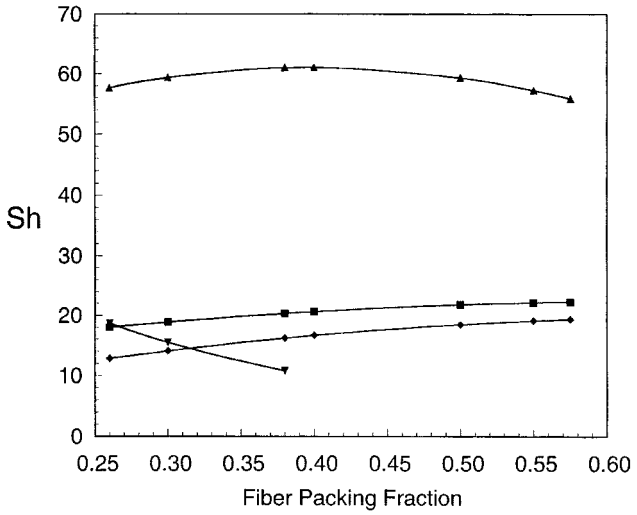

Figure 12. Dependence of Sh_{lm} on ϕ for $Re = 450$, $Sc = 1{,}000$, and $2R/L = 0.0039$ as predicted by various correlations.

◆—random packing, constant wall concentration; ■—square array; ▲—Costello et al. (1993); ▼—Prasad and Sirkar (1988); results for Yang and Cussler (1986) are not shown since $\phi > 0.26$.

As fiber packing increases, the ease with which fluid is distributed across the fiber bundle decreases, since viscous resistance to flow across the bundle increases faster than the viscous resistance to flow along the bundle. Prior work has shown that this results in a decrease in mass-transfer coefficient as more of the fluid tends to flow through the periphery of the fiber bundle (Lemanski and Lipscomb, 1995). One can rationalize such a dependence by noting that at the maximum fiber packing, where fibers are touching, all of the fluid must flow axially along the interface between the fiber bundle and the external case. This effect can be exaggerated if fiber packing at the bundle–case interface is poor and ''large'' flow channels are formed that run axially along the interface or such channels exist within the fiber bundle. Poor module performance has been attributed to such bypassing effects (Noda et al., 1979; Wickramasinghe et al., 1992; Seibert et al., 1993) and been observed experimentally (Varma, 1998). Consequently, module designs that lead to large cross-flow regions or secondary flows could produce higher than expected mass-transfer coefficients and performance could decrease with increasing fiber packing as these flows are suppressed. This is consistent with the literature results shown in Figures 11 and 12.

Note that designs that increase mass-transfer coefficients can lead to improved module performance. However, per-

formance is also dependent on how efficiently the driving force for mass transfer is utilized. For example, while mass-transfer coefficients are higher in crossflow than countercurrent flow, module performance can be poorer because the concentration difference driving force is not utilized as well. To evaluate the interaction between these factors, a performance model must be used that accounts for the interaction between flow and concentration changes throughout the module.

Differences between our results and the literature may also be attributable to correlation in fiber location within the bundle. Unit cells used to represent the bundle were generated assuming no correlation between the positions of individual fibers. One would expect changes in the fiber autocorrelation function to have a significant impact on the results. Unfortunately, autocorrelation functions are not usually reported.

Systematic deviations from random packing are of particular concern for commercial modules fabricated from fiber tows. In the manufacturing process, multiple fibers are spun from a single spinneret and processed as a group or tow. The tow is typically wound on a spindle, like a spool of fiber, for storage. As a result, fibers within a tow tend to stick together and the tow itself acts much like a single fiber. Therefore, one might expect tows to pack randomly when tows are combined to form a module. Moreover, since fibers within a tow also pack randomly, one might expect open regions within the fiber bundle to cluster around two characteristic length scales: the interfiber length scale (distance between fibers within a tow) and the intertow length scale. Large gaps between tows might persist along the fiber bundle to form channels that lead to fluid bypass, as discussed earlier. We could use the theoretical approach described here to examine such effects by using random sequential addition to place tows within the unit cell *and* then place fibers within tows. However, this is beyond the scope of the present work.

Conclusions

A theoretical analysis of entry mass transfer for axial flows through randomly packed fiber bundles is presented. In the entry mass-transfer limit, an analytic expression exists for the mass-transfer coefficient, in terms of the velocity gradient normal to the surface of each fiber, for both a constant wall concentration and wall flux boundary condition. The required velocity gradients are obtained by assuming the fiber bundle can be represented by a periodic unit cell and using the boundary-element method to solve the conservation-of-momentum equation inside this cell. The combination of the analytic solution for the mass-transfer coefficient and the solution of the conservation-of-momentum equation by the boundary element method provides a relatively simple and accurate method for dealing with the complex geometry of the problem.

Mass-transfer coefficients calculated for regular square and triangular arrays are in good agreement with results from numerical approximations and results calculated using the known analytic velocity field. Results for random fiber packing indicate that mass-transfer coefficients can decrease by 30%. Moreover, for a fixed fiber packing, the range of mass-transfer coefficients can be as large as 30% of the average value.

Experimental measurements of shell-side mass-transfer coefficients are in poor agreement with theoretical values for either regular or random fiber packings. We attribute these differences to deviations from the assumed axial-flow pattern. The departure from axial flow can be due to (1) the effects of shell entry/exit regions and nonparallel fibers in the bundle that promote transverse flow; (2) changes in the transverse and axial-flow resistance with fiber packing; and (3) correlations between fiber positions in the bundle, especially the presence of bypass channels at the interface between fiber bundle and the external case or within the bundle itself.

Given local fiber packing information, we believe one could combine local models of flow and mass transfer with global models of module performance (such as Lemanski and Lipscomb, 1995) to calculate overall module performance. The local analysis described here would provide the mass-transfer coefficient and flow-rate–pressure-drop relationships, as a function of fiber packing, that are required to determine overall module performance.

Acknowledgments

The authors gratefully acknowledge partial support of this project by the National Science Foundation through Grant CTS-9408414.

Notation

i = number of unit cell translations
j = number of unit cell translations
l = unit vector
X = coordinate value, m
Y = coordinate value, m
Z = coordinate value, m
α = coefficient in mass-transfer coefficient correlation
$\dot{\gamma}$ = velocity gradient, 1/s
θ = angular coordinate
σ = pitch to diameter ratio

Subscripts and superscripts

x = x-coordinate value
y = y-coordinate value

Literature Cited

Bird, R. B., W. E. Stewart, and E. N. Lightfoot, *Transport Phenomena,* Wiley, New York (1960).
Brebbia, C. A., J. C. F. Telles, and L. C. Wrobel, *Boundary Element Techniques,* Springer-Verlag, Berlin (1984).
Chen, V., and M. Hlavacek, "Application of Voronoi Tessellation for Modeling Randomly Packed Hollow-Fiber Bundles," *AIChE J.*, **40**, 606 (1994).
Costello, M. J., A. G. Fane, P. A. Hogan, and R. W. Schofield, "The Effect of Shell Side Hydrodynamics on the Performance of Axial Flow Hollow Fibre Modules," *J. Memb. Sci.*, **80**, 1 (1993).
Crowder, R. O., and E. L. Cussler, "Mass Transfer in Hollow-Fiber Modules with Non-Uniform Hollow Fibers," *J. Memb. Sci.*, **134**, 235 (1997).
Cussler, E. L., *Diffusion,* Cambridge Univ. Press, Cambridge (1997).
Deen, W. M., *Analysis of Transport Phenomena,* Oxford Univ. Press, New York (1998).
Elmore, S., and G. G. Lipscomb, "Analytical Approximations of the Effect of a Fiber Size Distribution on the Performance of Hollow Fiber Membrane Separation Devices," *J. Memb. Sci.*, **98**, 49 (1995).
Emersleben, O., "Das Darcyshe Filtergesetz," *Phys. Z.*, **26**, 601 (1925).
Happel, J., "Viscous Flow Relative to Arrays of Cylinders," *AIChE J.*, **5**, 174 (1959).

Ho, W. S., and K. K. Sirkar, eds., *Membrane Handbook*, Van Nostrand Reinhold, New York (1992).
Leal, L. G., *Laminar Flow and Convective Transport Processes*, Butterworth-Heinemann, Boston (1992).
Lemanski, J., and G. G. Lipscomb, ''Effect of Shell-Side Flows on Hollow-Fiber Membrane Device Performance,'' *AIChE J.*, **41**, 2322 (1995).
Lipscomb, G. G., ''Design of Hollow Fiber Contactors for Membrane Gas Separations,'' *The 1996 Membrane Technology Review*, Business Communications, Norwalk, CT (1996).
McBean, E. A., and F. A. Rovers, *Statistical Procedures for Analysis of Environmental Monitoring Data & Risk Assessment*, Prentice Hall, Upper Saddle River, NJ (1998).
Miyatake, O., and H. Iwashita, ''Laminar Flow Heat Transfer to a Fluid Flowing Axially Between Cylinders with a Uniform Surface Temperature,'' *Int. J. Heat Mass Transfer*, **33**, 417 (1990).
Miyatake, O., and H. Iwashita, ''Laminar Flow Heat Transfer to a Fluid Flowing Axially Between Cylinders with a Uniform Wall Heat Flux,'' *Int. J. Heat Mass Transfer*, **34**, 322 (1991).
Noda, I., and C. C. Gryte, ''Mass Transfer in Regular Arrays of Hollow Fibers in Countercurrent Dialysis,'' *AIChE J.*, **25**, 113 (1979).
Noda, I., D. G. Brown-West, and C. C. Gryte, ''Effect of Flow Maldistribution on Hollow Fiber Dialysis—Experimental Studies,'' *J. Memb. Sci.*, **5**, 209 (1979).
Prasad, R., and K. K. Sirkar, ''Dispersion-Free Solvent Extraction with Microporous Hollow-Fiber Modules,'' *AIChE J.*, **34**, 177 (1988).
Rogers, J. D., and R. L. Long, ''Modeling Hollow Fiber Membrane Contactors Using Film Theory, Voronoi Tessellations, and Facilitation Factors for Systems with Interface Reactions,'' *J. Memb. Sci.*, **134**, 1 (1997).
Seibert, A. F., X. Py, M. Mshewa, and J. R. Fair, ''Hydraulics and Mass Transfer Efficiency of a Commercial-Scale Membrane Extractor,'' *Sep. Sci. Technol.*, **28**, 343 (1993).
Sparrow, E. M., and L. A. Loeffler, ''Longitudinal Laminar Flow Between Cylinders Arranged in Regular Arrays,'' *AIChE J.*, **5**, 325 (1959).
Varma, A., ''Theoretical and Experimental Studies of the Influence of Dialysate Flow on Artificial Kidney Performance,'' Masters Thesis, Univ. of Toledo, Toledo, OH (1998).
Wickramasinghe, S. R., M. J. Semmens, and E. L. Cussler, ''Mass Transfer in Various Hollow Fiber Geometries,'' *J. Memb. Sci.*, **69**, 235 (1992).
Yang, M. C., and E. L. Cussler, ''Designing Hollow Fiber Contactors,'' *AIChE J.*, **32**, 1910 (1986).

Manuscript received Apr. 30, 1999, and revision received Aug. 9, 1999.